

This article has been published in The Journal of Chemical Physics 160, 164312 (2024), doi: 10.1063/5.0202573. The published version is available at: <https://pubs.aip.org/aip/jcp/article/160/16/164312/3284893/NH3-adsorption-and-competition-with-H2O-on-a>.

NH₃ adsorption and competition with H₂O on a hydroxylated aluminosilicate surface

Giada Franceschi,^{*1} Andrea Conti,¹ Luca Lezuo,¹ Rainer Abart,² Florian Mittendorfer,¹ Michael Schmid,¹ and Ulrike Diebold¹

¹Institute of Applied Physics, TU Wien, 1040 Vienna, Austria

²Department of Lithospheric Research, Universität Wien, 1090 Vienna, Austria

[*franceschi@iap.tuwien.ac.at](mailto:franceschi@iap.tuwien.ac.at)

Abstract

The interaction between ammonia (NH₃) and (alumino)silicates is of fundamental and applied importance, yet the specifics of NH₃ adsorption on silicate surfaces remain largely unexplored, mainly because of experimental challenges related to their electrically insulating nature. An example of this knowledge gap is evident in the context of ice nucleation on silicate dust, wherein the role of NH₃ for ice nucleation remains debated. This study explores the fundamentals of the interaction between NH₃ and microcline feldspar (KAlSi₃O₈), a common aluminosilicate with outstanding ice nucleation abilities. Atomically resolved non-contact atomic force microscopy, X-ray photoelectron spectroscopy, and density functional theory-based calculations elucidate the adsorption geometry of NH₃ on the lowest-energy surface of microcline, the (001) facet, and its interplay with surface hydroxyls and molecular water. NH₃ and H₂O are found to adsorb molecularly in the same adsorption sites, creating H-bonds with the proximate surface silanol (Si-OH) and aluminol (Al-OH) groups. Despite the closely matched adsorption energies of the two molecules, NH₃ readily yields to replacement by H₂O, challenging the notion that ice nucleation on microcline proceeds via the creation of an ordered H₂O layer atop pre-adsorbed NH₃ molecules.

Key words: NH₃, AFM, surface acidities, aluminosilicate, hydroxyls

Introduction

Ammonia (NH_3) adsorption on solid surfaces is a matter of intense applied and fundamental research. It is integral to environmental and industrial processes such as NH_3 capture for air pollution reduction, NH_3 -based fertilizer production, hydrogen storage, and environmental chemistry.¹ Moreover, NH_3 is abundant in space, and its adsorption on interstellar grains is studied to glean insights into the nitrogen chemistry of the interstellar medium, thought to occur predominantly via gas-grain reactions.² Fundamentally, NH_3 adsorption processes are regulated by acid-base reactions between different surface sites and NH_3 . Because of the exquisite sensitivity of NH_3 adsorption to the local properties of the surface, adsorption of NH_3 is often used to probe the strength and distribution of surface acidic sites.³ On oxide surfaces, NH_3 binding can occur in three main ways: via the lone pair of its N atom to a cation that acts as a Lewis acid; by H-bonding via one of its H atoms to a surface O atom; or by H-bonding via its N atom to an H atom of surface hydroxyl groups (OH). Other feasible ways of ammonia adsorption involve the complete proton transfer from a Brønsted site to create NH_4^+ , or NH_3 dissociation into NH_2 (or NH) and OH species.⁴

To ensure a uniform collection of adsorption sites, NH_3 adsorption studies are ideally conducted on atomically controlled single crystals prepared under ultra-high vacuum (UHV). To date, these types of studies have been limited to metals^{5–8} and various polymorphs of TiO_2 ,^{9–13} where NH_3 tends to adsorb molecularly on Ti sites via its N lone pair, although dissociation was observed after electron bombardment or on defective surfaces.^{9,12} On the other hand, investigations on important materials for NH_3 capture, such as metal-organic frameworks (MOFs) and (alumino)silicates, are typically conducted with porous or amorphous samples.^{14–16} In such heterogeneous systems, data interpretation becomes challenging due to surface defects, hydroxyls, or ill-defined atom surroundings that can affect local acidities.^{12,17} In aluminosilicates, further complexity is given by the details of their Si-Al framework: the specific distribution of Al ions can affect the heat of adsorption of NH_3 .^{16,18} Another important factor is humidity and the water contents of the sample; this can affect NH_3 adsorption through cooperative¹⁹ or competitive^{20,21} effects between NH_3 and H_2O , potentially leading to NH_3 replacement by H_2O even when the adsorption energy of NH_3 is stronger than that of H_2O .²⁰ To explore the fundamentals of NH_3 adsorption and its interplay with H_2O on complex systems such as aluminosilicates, well-defined model systems in the form of atomically characterized single crystals investigated under pristine conditions are helpful.

The importance of understanding the details of NH_3 adsorption on aluminosilicates and its interplay with H_2O extends to current atmospheric research on ice nucleation (IN) on mineral dust, an important phenomenon affecting the glaciation of clouds with implications for Earth's climate. K-feldspars, particularly the microcline polymorph (KAlSi_3O_8), are crucial IN agents. Microcline's exceptional IN activity^{22–29} is generally rationalized through two main perspectives: one emphasizing surface chemistry, which would promote the formation of H-bonded H_2O networks,^{30,31} and the other focusing on composition and structural heterogeneities or defects.^{32–35} Another important factor is atmospheric chemistry. While travelling in the atmosphere, mineral dust particles are often embedded within aqueous liquid droplets, which can induce preferential dissolution,^{36–38} chemical coatings,³⁹ or net surface charges^{40,41} – all of which can impact ice formation. Specifically, it was found that IN activities are substantially

enhanced in the presence of dilute NH_3 - and NH_4^+ -containing solutions.⁴²⁻⁴⁴ However, the underlying reasons are debated. Current interpretations revolve around the replacement of K^+ ions by NH_3 or NH_4^+ as well as their adsorption on the surface, which may offer oriented H bonds for ice growth,^{40,42,44,45} and the nature of NH_4^+ ions, which may replace H_2O within the ice network, increasing the configurational entropy of ice and decreasing its overall free energy.^{46,47} Experimental investigations on NH_3 adsorption on microcline single crystals and its potential interplay with H_2O may enable testing these hypotheses.

This work explores the fundamentals of the interaction of ammonia with microcline feldspar as a prototypical hydroxylated aluminosilicate. Crystalline microcline samples were cleaved in UHV to expose the lowest-energy (001) surface and investigated by atomically resolved non-contact atomic force microscopy (AFM), X-ray photoelectron spectroscopy (XPS), complemented by density functional theory (DFT) calculations. By depositing controlled amounts of NH_3 and H_2O molecules at 100 K on microcline (001), it is found that NH_3 adsorbs molecularly by creating H bonds with its surface silanol (Si-OH) and aluminol (Al-OH) groups, occupying the same adsorption site as H_2O with an adsorption energy reaching almost that of H_2O . When H_2O is deposited onto the surface with pre-adsorbed ammonia, it partially replaces the adsorbed NH_3 molecules rather than creating H-bonded networks with the ammonia layer.

Materials and methods

The experiments were carried out in a UHV setup consisting of two interconnected chambers: A preparation chamber for sample cleaving and XPS (base pressure below 1×10^{-10} mbar), and an adjacent chamber for AFM (1×10^{-11} mbar). A natural microcline feldspar from Russia (from Priv.-Doz. Uwe Kolitsch, Natural History Museum Vienna) was characterized *ex situ* as detailed elsewhere.³¹ (001)-oriented grains from the main crystal were mounted onto Omicron-style stainless-steel sample plates and cleaved in the preparation chamber.³¹ After cleaving, the samples exhibited strong surface charges, as also observed on other cleaved insulators.⁴⁸ To remediate such charge, the samples were irradiated for one minute with X-rays from the XPS setup.

Water (ultrapure deionized water, milliQ[®], further purified through three freeze-pump-thaw cycles) and anhydrous ammonia (Linde, 99.999%) were dosed from leak valves while keeping the sample holder on the preparation chamber's manipulator at 100 K. The number of molecules deposited is always expressed with respect to the primitive unit cell of the hydroxylated surface (u.c.; 0.55 nm^2). The calibration is based on the amount (partial pressure \times time) needed to obtain a coverage of 1 molecule/u.c. as judged by AFM, assuming 100% sticking probability. Warming up the sample to room temperature caused the desorption of all H_2O and NH_3 molecules from the hydroxylated surface, as evidenced by XPS and AFM.

XPS was performed with a non-monochromatic dual-anode Mg/Al X-ray source (SPECS XR 50) and a hemispherical analyzer (SPECS Phoibos 100). Spectra were acquired in grazing emission (70° from the surface normal). The intensities and positions of the Al-K α -excited XPS peaks were evaluated with CasaXPS after subtracting a Shirley-type background. For the display and analysis of the XPS data, an energy correction was applied to all spectra to compensate for the charging of the electrically insulating sample: The Si 2*p* core-level peak was set to 103.10 eV, as reported in the literature.⁴⁹ Fitting procedures and parameters are

reported in Section S3. XPS was used to obtain an approximate desorption temperature for NH_3 . A nominal coverage of 5 NH_3 molecules/u.c. was deposited on the UHV-cleaved sample at 100 K. The amount was calibrated based on the dose (pressure \times time) needed to observe one NH_3 molecule/u.c. in AFM, assuming 100% sticking probability. The sample was warmed to increasingly higher temperatures in steps of 10 K, and XPS spectra (N 1s, O 1s, K 2p, and Si 2p for energy correction) were acquired at each stage. The coverage of the molecular NH_3 roughly halved at a temperature between 150 K and 160 K.

The AFM measurements were performed at 4.7 K using a commercial Omicron qPlus LT head and a differential cryogenic amplifier,⁵⁰ in constant-height mode. The qPlus AFM sensors ($k = 2000\text{--}3500$ N/m, $f_0 \approx 32$ kHz, $Q \approx 50000$) had a separate contact for the tunneling current. Before each measurement, the tips were prepared on an oxygen-exposed Cu(110) single crystal by repeated indentation and voltage pulses. CuO_x -terminated tips were prepared on the oxygen-induced reconstruction of Cu(110)⁵¹ to exhibit a frequency shift smaller than -1.5 Hz. Local contact potential difference (LCPD) measurements by the Kelvin parabola method⁵² were performed to assess residual fields. Residual surface charges were compensated by applying a bias voltage V_s to the back of the sample plate while keeping the tip potential close to the ground.

DFT calculations were performed with the Vienna Ab-initio Simulation Package (VASP)^{53,54} using the $r^2\text{SCAN-D3}$ metaGGA exchange-correlation functional.⁵⁵ Details about the bulk optimization, unit cell, geometries, cutoff energies, and convergence criteria are specified elsewhere.³¹ The AFM images were simulated with the Probe Particle Model,^{56,57} which includes Hartree-potential electrostatics and Lennard-Jones potentials as well as the elastic properties of the tip based on the methods described in Refs. ^{56,57}. CuO_x tips were simulated with the following values of lateral and vertical spring constants and charges: $k_{x,y} = 161.9$ N/m, $k_z = 271.1$ N/m, effective tip charge of $-0.05e$. The oscillation amplitude for each simulation always matched the one used in the corresponding experimental image. Since the exact height of the tip is not known, simulated AFM images were calculated for different tip heights; the displayed simulated image is the one fitting the experiment best. Tip-sample distances are always referenced to the most protruding surface atom.

Results

Previous studies have shown that microcline (001) readily hydroxylates.³¹ Even when the sample was cleaved in UHV, the water entrapped in the mineral, and freed during the cleave, is sufficient to create a fully hydroxylated layer that was stable at room temperature.³¹ Thus, the starting point of all experiments in this paper was a hydroxylated surface. As shown in Figs. 1a, d, such a layer consists of an ordered array of silanol (Si-OH) and aluminol (Al-OH) groups. When water is dosed below 150 K onto the hydroxylated surface, it adsorbs molecularly at well-defined sites, i.e., in between adjacent silanol and aluminol groups – accepting an H bond from the silanol, and donating one to the aluminol.³¹ Figures 1b, e show the DFT-optimized model and the experimental AFM images obtained for a coverage of one H_2O molecule per unit cell (in addition to the dissociated H_2O of the hydroxylated surface in Fig. 1a). In experiments performed with CuO_x tips,⁵¹ the appearance of the water species is very sensitive to the tip-sample distance (Fig. S1a–d). At large distances, H_2O appears with a

positive frequency shift (bright); as the tip approaches closer, dark, isolated features suddenly appear. These dark features have a rather sharp boundary and a bright rim, as seen in Fig. 1b.

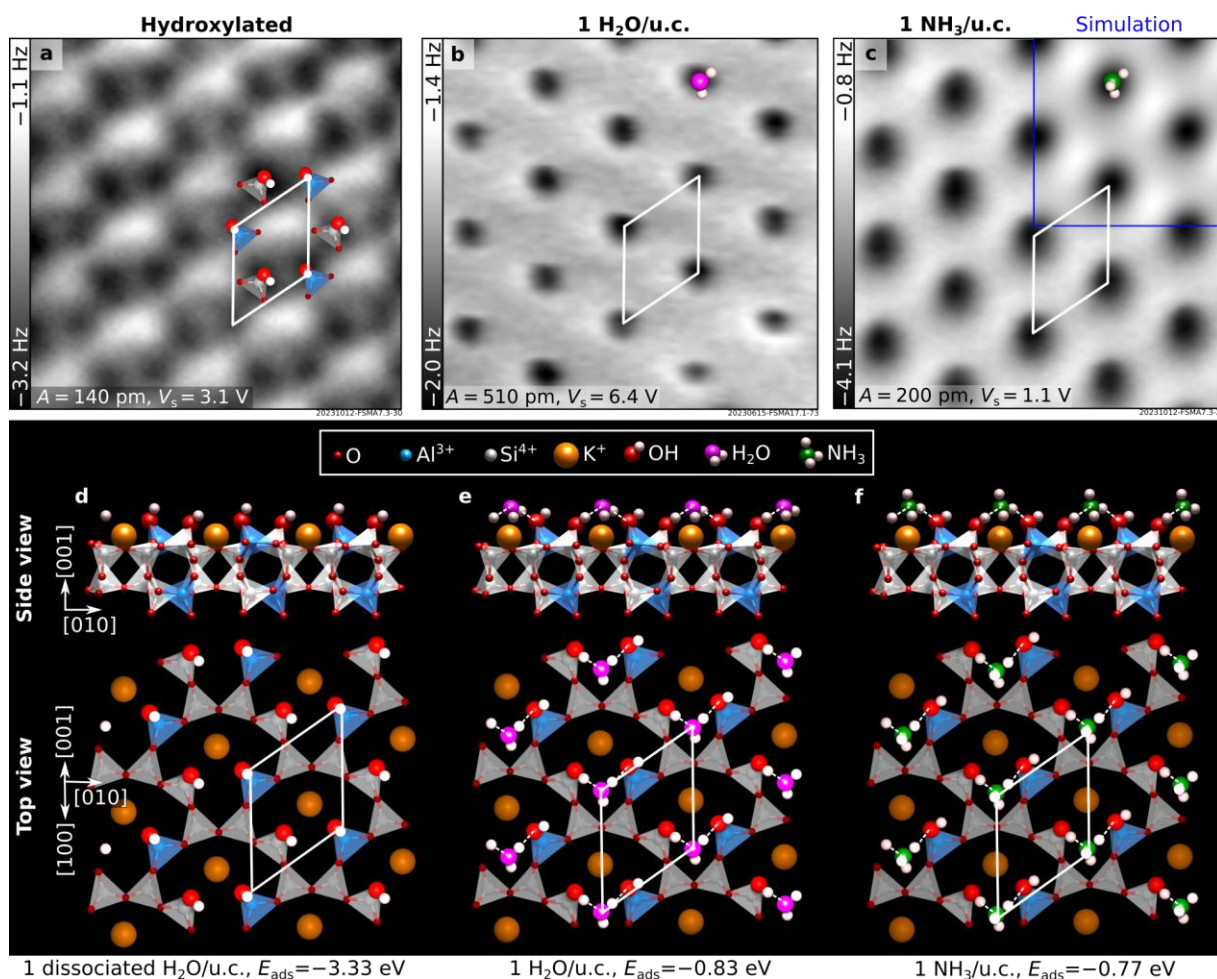


Figure 1. H₂O and NH₃ adsorption on microcline (001). (a–c) $3.2 \times 3.2 \text{ nm}^2$ AFM images of the hydroxylated, H₂O-, and NH₃-exposed microcline (001) surface acquired with CuO_x tips.⁵¹ H₂O and NH₃ were deposited at 100 K onto the hydroxylated surface to reach a coverage of one molecule per unit cell (u.c.). (d–f) Corresponding DFT models. SiO₄ tetrahedra are gray, AlO₄ tetrahedra blue. Panels (d, e) are adapted from Ref. ³¹. The AFM simulation obtained from the model in panel (f) is shown in the inset of panel (c); acquired at a tip–sample distance of $d = 5.5 \text{ \AA}$. White rhombi identify primitive unit cells. Calculated adsorption energies (E_{ads}) are reported below the corresponding models.

Dosing NH₃ below 150 K onto the hydroxylated microcline surface produces a similar structure as the water-exposed one for comparable coverages (Fig. 1c). One dark feature per unit cell is visible, appearing larger and smoother than those caused by H₂O molecules and producing a more gradual frequency change as a function of the tip–sample distance (for a comparison of images of the NH₃ and H₂O taken with the same tip, see Fig. S1). Figure 1f presents the lowest-energy structure found for one adsorbed NH₃ molecule per unit cell. An intact NH₃ occupies the same adsorption site as H₂O. The calculated NH₃ adsorption energy (E_{ads}) is only marginally lower than for H₂O (-0.77 eV vs. -0.83 eV), consistent with the similar desorption temperature of H₂O and NH₃ (between 150 K and 160 K, as inferred from XPS – see Methods). Like H₂O, NH₃ accepts an H bond from a silanol group while donating one to the adjacent aluminol group. One of the two remaining H atoms points away from the surface; the other one lies within the surface and points in the same direction as the free H atom

of adsorbed H₂O. The corresponding AFM simulation, superimposed on the experimental image of Fig. 1c, reproduces the experimental contrast.

In XPS, the N 1s peak measured on a surface covered by 1 NH₃/u.c. sits at 400.4 eV XPS binding energy after correction for charging³¹ (see Section S3 for details). The peak intensity increases with ammonia deposition at 100 K while preserving its position and width until the nominal amount of ≈ 3 NH₃/u.c., after which the intensity saturates (see Section S3). This suggests that multilayer adsorption is possible only below 100 K, consistent with previous temperature programmed desorption studies on crystalline forsterite (Mg₂SiO₄)² and TiO₂,¹³ which observed the multilayer NH₃ desorption peak around 100 K. Warming up the NH₃-covered sample to room temperature causes the intensity to decrease and leads to the eventual disappearance of the N 1s peak without the formation of any shoulders, suggesting that NH₃ desorbs from the surface as an intact molecule.

To test whether adsorbed NH₃ can serve as a template for an ordered and oriented layer of water ice, H₂O was deposited at 100 K on the NH₃-saturated surface of Figs. 1c, f. In XPS (Fig. 2a), the H₂O component of the O 1s peak (black) increases as a function of the H₂O coverage, as expected. However, the increase is significantly smaller than when H₂O is deposited directly on the hydroxylated surface (grey), indicating that fewer H₂O molecules stick to the surface with pre-adsorbed NH₃. (While this could also indicate that 3D clusters are formed, which contribute less to the XPS intensity, the AFM data discard this hypothesis.). At the same time, the N 1s signal (green) decreases. Figures 2b–d show the evolution of selected N 1s and the O 1s peaks (see Section S3 for details about the fitting procedures).

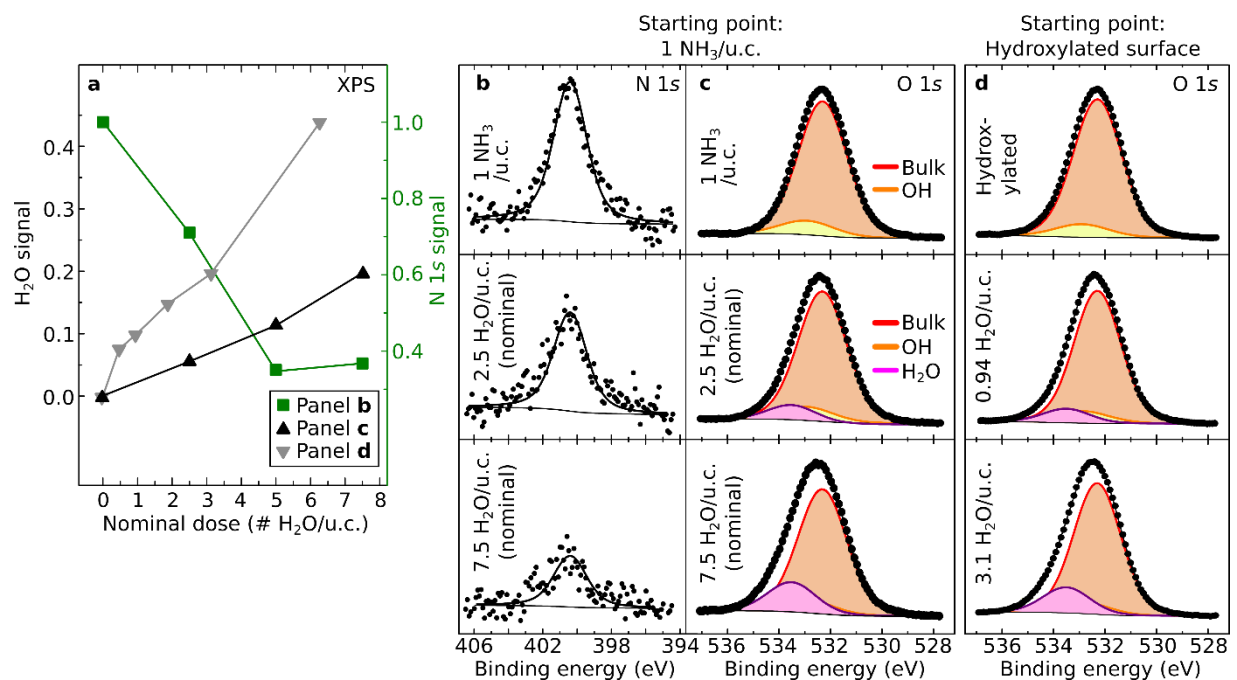


Figure 2. Substitution of NH₃ by H₂O measured with XPS. (a) XPS signals as a function of nominal H₂O dose, for adsorption at 100 K onto an NH₃-exposed surface (green, squares: N 1s, black, upward-pointing triangles: H₂O component of O 1s), and over a hydroxylated surface without NH₃ (grey, downward-pointing triangles: H₂O component of O 1s). N 1s counts are normalized to the peak area obtained for 1 NH₃/u.c.; H₂O areas are normalized to the O 1s bulk component of the O 1s peak before any H₂O exposure. Error bars on the intensities are comparable to the symbol sizes. The nominal doses do not account for intrinsic errors due to pumping by the chamber walls. Lines connecting symbols are meant to guide the eye. (b–d) Evolution of selected N 1s and O 1s spectra with corresponding fittings. Nominal H₂O doses are noted at the sides of the corresponding panels. For all

spectra: Al K α , 1486.61 eV, pass energy 20 eV, 70° grazing emission. Binding energy axes were adjusted to account for charging (see Methods). The O 1s peak was fit as described in Section S3.

The AFM images in Fig. 3 help interpreting the XPS trends. Dosing a nominal amount of 2.5 H₂O/u.c. onto the surface with pre-adsorbed NH₃ produces the surface shown in Fig. 3a. Most of it appears as light-gray areas with weak modulations of Δf . When imaged at closer tip-sample distances (Fig. 3d), these areas have the same appearance as the hydroxylated surface with a mixture of H₂O and NH₃ molecules (compare with Figs. 1b, c). Similar to the case of single-molecule adsorption, it is evident that also in the mixed phase the H₂O and NH₃ molecules occupy the same site of the unit cell. The deposited H₂O has substituted $\approx 40\%$ of the pre-adsorbed NH₃ molecules. In addition to the areas of coexisting NH₃ and H₂O, a few isolated darker dots are visible in Fig. 3a. Darker contrast indicates a stronger attractive interaction with the AFM tip during the constant-height image acquisition. It is attributed to water species deposited on top of the mixture of NH₃ and H₂O, thus sticking out further from the surface. In the top part of Fig. 3a, imaged at a closer tip-sample distance in Fig. 3e, a cluster of such darker features is visible. This cluster resembles what is observed by dosing H₂O directly onto the hydroxylated surface without any pre-adsorbed NH₃ (Section S2). However, in the absence of pre-adsorbed NH₃, the water islands are significantly larger for comparable gas doses, consistent with the higher H₂O signals measured in XPS (Fig. 2a). Additionally, the water islands resulting from deposited water only display internal short-range ordering; such ordering is instead absent in the water islands of Fig. 3.

The water islands grow bigger with increasing water coverages, see Figs. 3b, c, where the nominal gas doses correspond to 5 H₂O and 7.5 H₂O/u.c., respectively. In Fig. 3b, the water islands occupy almost the whole surface (the dark dots are not so well resolved as in Fig. 3a because the image is acquired with the tip further away from the surface). A few small, bright patches remain where H₂O and NH₃ coexist, two of which are marked. In Fig. 3c, the surface is fully covered by the protruding water islands; several dark spots with different attractive contrast and without any long-range ordering are visible. In XPS (Fig. 2a), the NH₃ signal has reached its minimum already at the nominal gas dose of 5 H₂O/u.c., indicating that H₂O replaces NH₃ only to a certain extent. Thus, H₂O grows atop the mixed layer of NH₃ and H₂O. Note that it cannot be excluded that a small fraction of NH₃ molecules participate to the growth of the water islands mentioned above.

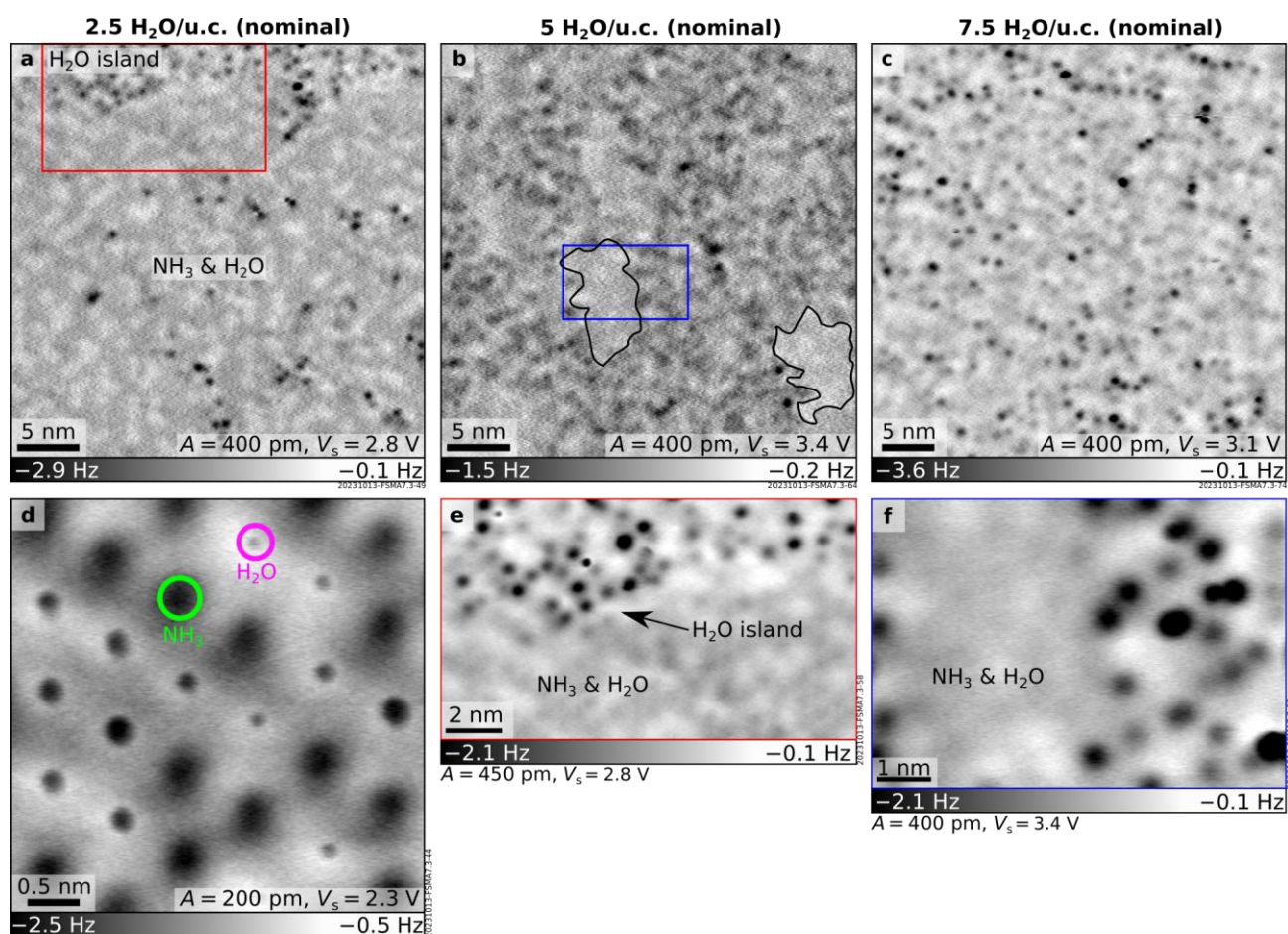


Figure 3. Substitution of NH_3 by H_2O , AFM. (a–f) AFM images of a surface exposed to NH_3 at 100 K (gas dose corresponding to 1 molecule per unit cell, as in Figs. 1c, f), followed by H_2O exposure. (a, d, e) Nominal gas dose of 2.5 $\text{H}_2\text{O}/\text{u.c.}$. (a) The majority of the surface appears as a mixture of H_2O and NH_3 , as seen in more detail in panel (d). The top portion of panel (a), imaged at a closer tip-sample distance in panel (e), evidences the growth of additional H_2O . (b, f) Nominal gas dose of 5 $\text{H}_2\text{O}/\text{u.c.}$: The surface is almost fully covered by H_2O islands. Small patches remain in which adsorbed H_2O and NH_3 coexist, two of which are marked by dark outlines. The area marked by the blue rectangle is imaged at a closer tip-sample distance in panel (f). (c) Nominal gas dose of 7.5 $\text{H}_2\text{O}/\text{u.c.}$: The surface is fully covered by a disordered H_2O layer.

Discussion

Molecular insights into NH_3 adsorption.

The (001) surface investigated here is the lowest-energy facet of microcline. Thus, it is likely that this surface is also exposed by mineral dust particles. It serves as a model system to investigate the adsorption mechanisms of gas-phase ammonia and water on hydroxylated aluminosilicate surfaces. The data reveal that NH_3 deposited below 150 K adsorbs molecularly via H bonds with the available surface hydroxyls. It is reasonable for molecular adsorption to prevail over the formation of NH_4^+ ions or NH_3 dissociation upon adsorption. The strong energy gain associated with surface hydroxylation (adsorption energy of ≈ -3.3 eV/ H_2O , see Fig. 1b³¹) outweighs the interaction between NH_3 and the hydroxyl groups (adsorption energy of ≈ -0.8 eV, see Fig. 1c), making the transfer of protons from silanols to NH_3 to create NH_4^+ unlikely. The situation could be different in solution, however, where the ready availability of

protons may stabilize NH_4^+ ions while maintaining the surface hydroxyls. NH_3 dissociation is also not expected because of the lack of available surface O sites that would accept a proton.

The NH_3 molecule acts as both a H-bond acceptor and H-bond donor in the adsorption configuration on microcline. According to the general expectation, NH_3 should accept H bonds from surface OH groups by forming an H bond between its N atom and the H atom of the OH group.^{4,21} Because of the favorable geometry of surface hydroxyls on the hydroxylated microcline surface, NH_3 here exhibits amphoteric behavior with respect to H bonds: The NH_3 molecule engages with two proximate OH groups by accepting an H-bond from the silanol and donating one to the aluminol. The individual behaviors of silanols (H-bond donating) and aluminols (H-bond accepting) are determined by their coordination chemistry: The larger charge of silicon compared to aluminum (oxidation state +4 vs. +3) strengthens the Si-OH bond relative to the Al-OH bond, making it easier to release H from Si-OH than from Al-OH. These considerations equally apply to the adsorption of H_2O , which occupies the same site as NH_3 and interacts with proximate OH groups in a similar manner.³¹

The results demonstrate the significance of the atomic environment in determining the acidity of surface hydroxyls, as already predicted by previous computational studies on amorphous silica, where variations in the exact coordination and atomic environment lead to distinct acid behaviors even for the same hydroxyl type.^{15,17,58} Extending these reasonings to aluminosilicates, one expects that the relative density and distribution of aluminol and silanol groups (and thus, of Si and Al ions in the Si-Al framework) will affect local acidities. Consistently, zeolites and mesoporous silica evidence changes in heats of adsorption for NH_3 and acidity in response to alterations in Al concentrations and distributions.^{16,18,59} Therefore, accurate acidity measurements on aluminosilicate surfaces necessitate careful consideration of the distribution and geometric proximity of aluminols and silanols. In this respect, other terminations of microcline besides the (001) surface investigated here, as well as other polymorphs exposing surfaces with different arrangements of silanol and aluminol groups, are expected to produce adsorption configurations of ammonia and water differing from those reported here.

Interplay between NH_3 and H_2O and implications for atmospheric ice nucleation.

Figures 2 and 3 illustrate how a hydroxylated surface pre-dosed with NH_3 changes after exposure to H_2O at low temperatures. H_2O does not simply adsorb atop NH_3 . Instead it tends to substitute adsorbed NH_3 , as judged from the coexistence of H_2O and NH_3 at equivalent adsorption sites seen in Figs. 3a, d and by the XPS trends of Fig. 2a. For comparable H_2O doses, the H_2O signals are larger for the hydroxylated surface without NH_3 compared to the NH_3 -pre-adsorbed one, suggesting that H_2O sticks less to the latter. Such sticking effects are likely due to the competition of H_2O and NH_3 to adsorb on the same site, which promotes the substitution of the adsorbed species over H_2O growth atop NH_3 . A chemical interaction of H_2O with NH_3 is deemed unlikely. If one of the H atoms of H_2O were to interact with NH_3 to transform it, e.g., to NH_4^+ , a shift of ≈ 2 eV in the N 1s peak would be expected,⁶⁰ which is not present here. Moreover, an attractive interaction between H_2O and NH_3 would favor NH_3 to remain on the surface. On the contrary, the NH_3 signal decreases with increasing H_2O dose.

This indicates that NH_3 and H_2O compete for adsorption sites and speaks against a strong binding between them.

Notably, the substitution occurs despite the minimal energy differences in the adsorption energies of H_2O and NH_3 predicted by DFT (-0.83 eV vs. -0.77 eV). Similar effects have been previously observed within MOF cages,²⁰ where NH_3 molecules bound to metal centers can be readily substituted by H_2O even when NH_3 has significantly stronger adsorption energies. This behavior was attributed to cooperative effects between the H_2O molecules as well as a strong interaction between H_2O and NH_3 , which can weaken the bond between NH_3 and the metal center while reducing the kinetic barriers to perform the substitution. Similarly, incoming H_2O molecules onto the microcline surface with pre-adsorbed NH_3 may interact with the adsorbed NH_3 via H-bonding, weakening the bond between NH_3 and the surface OH and eventually leading to its detachment. After $\approx 40\%$ of NH_3 has been substituted by H_2O , H_2O islands grow atop the mixed NH_3 - H_2O layer.

The current investigation contributes to ongoing discussions on atmospheric IN on microcline and the role of ammonia in this process. The mechanisms leading to enhanced IN activities of microcline upon immersion in ammonia solutions⁴²⁻⁴⁴ are currently debated. Some studies emphasize the role of the direct adsorption of NH_3 or NH_4^+ to the surface hydroxyls.⁴² In this case, the oriented, extra protons offered by the adsorbed NH_3 molecules should favor the formation of ordered H-bonded networks and thus facilitate IN.^{40,42,45} This picture is supported by sum frequency generation studies on silica surfaces, indicating that adsorbed NH_3 enforces a net orientation of H_2O molecules at the ice-silica interface.⁴⁵ The present study shows that, during gas-phase interaction under UHV conditions, H_2O does not orderly bind on top of a layer of adsorbed NH_3 . Instead, the two species compete for the same adsorption sites, leading to a partial replacement of NH_3 by H_2O . In the atmosphere, NH_3 has a drastically lower concentration than H_2O , existing in the parts per billion. Under the oversimplified assumption of gas-phase interactions between microcline and the two substances in the atmosphere, one expects H_2O adsorption to prevail over NH_3 because of the concentration difference of the two species and their comparable binding energies. Thus, in this context, the mere adsorption of water over ammonia can be ruled out as a dominant factor for increased IN activities. However, the situation will be different in liquid and thick ice layers. Effects proposed in the literature, such as pH-dependent surface charge, ion exchange (K^+ for NH_4^+),⁴⁴ or preferential dissolution, may dominate. Moreover, some studies suggest that the effect of ammonia solutions is related to the peculiar properties of the NH_4^+ ions: NH_4^+ is prone to replace H_2O within the ice network while offering an additional proton for H bonding, increasing the configurational entropy of the ice structure and thus lowering its free energy.^{46,47}

Conclusions

This work sheds light on the molecular-scale interaction of gaseous NH_3 with a prototypical aluminosilicate, particularly one prone to hydroxylation upon exposure to water vapor. Based on the phase diagram in Ref. ³¹, the surface of microcline (001) should be hydroxylated (as in Fig. 1a) under ambient conditions as well. The stability of the hydroxylated surface makes it pertinent for fundamental investigations of environmental processes such as atmospheric ice nucleation. Through atomically resolved AFM imaging and DFT-based calculations, it was found that NH_3 adsorbs molecularly on hydroxylated microcline feldspar (001) by H-bonding

to its surface aluminol and silanol groups. The geometric proximity and coordination chemistry of the two hydroxyl groups determine the specific adsorption configuration of NH₃, which acts as both H-bond donor and H-bond acceptor. The intimate link between the adsorption geometry of NH₃ and the type and distribution of surface OH groups evidenced here stresses the importance of determining the distribution of surface Si and Al tetrahedra for reliable acidity measurements of aluminosilicates. When water is introduced onto the surface with pre-adsorbed NH₃, it competes for the same adsorption sites, leading to partial replacement and precluding the growth of ordered water networks over adsorbed NH₃.

Conflicts of interest

There are no conflicts to declare.

Data Availability

The data that support the findings of this study are available from the corresponding author upon reasonable request.

Acknowledgements

This work was supported by the European Research Council (ERC) under the European Union's Horizon 2020 research and innovation programme (grant agreement No. 883395, Advanced Research Grant 'WatFun'). The computational results presented have been achieved using the Vienna Scientific Cluster (VSC). Priv-Doz. Uwe Kolitsch from the Natural History Museum Vienna is acknowledged for providing the samples used for this work.

Appendix A. Supplementary Material

Section S1: AFM images at different tip-sample distances. Section S2: Dosing H₂O directly on the hydroxylated surface. Section S3: XPS spectra.

References

- (1) Han, B.; Butterly, C.; Zhang, W.; He, J. Z.; Chen, D. Adsorbent Materials for Ammonium and Ammonia Removal: A Review. *J. Clean. Prod.* **2021**, *283*, 124611. <https://doi.org/10.1016/j.jclepro.2020.124611>.
- (2) Suhasaria, T.; Thrower, J. D.; Zacharias, H. Thermal Desorption of Ammonia from Crystalline Forsterite Surfaces. *Mon. Not. R. Astron. Soc.* **2015**, *454* (3), 3317–3327. <https://doi.org/10.1093/mnras/stv2197>.
- (3) Gervasini, A.; Auroux, A. Microcalorimetric Investigation of the Acidity and Basicity of Metal Oxides. *J. Therm. Anal.* **1991**, *37* (8), 1737–1744. <https://doi.org/10.1007/BF01912203>.
- (4) Tsyganenko, A. A.; Pozdnyakov, D. V.; Filimonov, V. N. Infrared Study of Surface Species Arising from Ammonia Adsorption on Oxide Surfaces. *J. Mol. Struct.* **1975**, *29* (2), 299–318. [https://doi.org/10.1016/0022-2860\(75\)85038-1](https://doi.org/10.1016/0022-2860(75)85038-1).
- (5) Klauber, C.; Alvey, M. D.; Yates, J. T. NH₃ Adsorption on Ni(110) and the Production of the NH₂ Species by Electron Irradiation. *Surf. Sci.* **1985**, *154* (1), 139–167. [https://doi.org/10.1016/0039-6028\(85\)90359-0](https://doi.org/10.1016/0039-6028(85)90359-0).
- (6) Madey, T. E.; Benndorf, C. Influence of Surface Additives (Na and O) on the Adsorption and Structure of NH₃ on Ni(110). *Surf. S* **1985**, *153*, 587–595. [https://doi.org/10.1016/0039-6028\(85\)90191-8](https://doi.org/10.1016/0039-6028(85)90191-8).
- (7) Kay, B. D.; Lykke, K. R.; Creighton, J. R.; Ward, S. J. The Influence of Adsorbate–Absorbate Hydrogen Bonding in Molecular Chemisorption: NH₃, HF, and H₂O on Au(111). *J. Chem.*

- Phys.* **1989**, *91* (8), 5120–5121. <https://doi.org/10.1016/j.apsusc.2004.05.136>.
- (8) Xu, C.; Goodman, D. W. Adsorption of Ammonia and Its Influence on Coadsorbed Carbon Monoxide on Monolayer and Multilayer Palladium Epitaxially Grown on Mo(110). *J. Phys. Chem. B* **1998**, *102* (22), 4392–4400. <https://doi.org/10.1021/jp981054m>.
 - (9) Diebold, U.; Madey, T. E. Adsorption and Electron Stimulated Desorption of NH₃/TiO₂(110). *J. Vac. Sci. Technol. A Vacuum, Surfaces, Film.* **1992**, *10* (4), 2327–2335. <https://doi.org/10.1116/1.577939>.
 - (10) Koust, S.; Adamsen, K. C.; Kolsbjerg, E. L.; Li, Z.; Hammer, B.; Wendt, S.; Lauritsen, J. V. NH₃ Adsorption on Anatase-TiO₂(101). *J. Chem. Phys.* **2018**, *148*, 124704. <https://doi.org/10.1063/1.5021407>.
 - (11) Wilson, J. N.; Idriss, H. Reactions of Ammonia on Stoichiometric and Reduced TiO₂(001) Single Crystal Surfaces. *Langmuir* **2004**, *20* (25), 10956–10961. <https://doi.org/10.1021/la0484422>.
 - (12) Bühlmeier, H.; Adamsen, K. C.; Xu, T.; Lammich, L.; Libuda, J.; Lauritsen, J. V.; Wendt, S. Adsorption and Reaction of NH₃ on Rutile TiO₂(110): An STM Study. *J. Phys. Chem. C* **2022**, *126* (15), 6590–6600. <https://doi.org/10.1021/acs.jpcc.2c01414>.
 - (13) Kim, B.; Li, Z.; Kay, B. D.; Dohnálek, Z.; Kim, Y. K. The Effect of Oxygen Vacancies on the Binding Interactions of NH₃ with Rutile TiO₂(110)-1 × 1. *Phys. Chem. Chem. Phys.* **2012**, *14* (43), 15060–15065. <https://doi.org/10.1039/c2cp42754k>.
 - (14) Blomfield, G. A.; Little, L. H. Chemisorption of Ammonia on Silica. *Can. J. Chem.* **1973**, *51*, 1771–1781. <https://doi.org/10.1007/BF00855649>.
 - (15) Jystad, A. M.; Biancardi, A.; Caricato, M. Simulations of Ammonia Adsorption for the Characterization of Acid Sites in Metal-Doped Amorphous Silicates. *J. Phys. Chem. C* **2017**, *121* (40), 22258–22267. <https://doi.org/10.1021/acs.jpcc.7b08113>.
 - (16) Kapustin, G. I.; Brueva, T. R.; Klyachko, A. L.; Beran, S.; Wichterlova, B. Determination of the Number and Acid Strength of Acid Sites in Zeolites by Ammonia Adsorption. Comparison of Calorimetry and Temperature-Programmed Desorption of Ammonia. *Appl. Catal.* **1988**, *42* (2), 239–246. [https://doi.org/10.1016/0166-9834\(88\)80005-8](https://doi.org/10.1016/0166-9834(88)80005-8).
 - (17) Pfeiffer-Laplaud, M.; Costa, D.; Tielens, F.; Gageot, M. P.; Sulpizi, M. Bimodal Acidity at the Amorphous Silica/Water Interface. *J. Phys. Chem. C* **2015**, *119* (49), 27354–27362. <https://doi.org/10.1021/acs.jpcc.5b02854>.
 - (18) Zhakisheva, B.; Gutiérrez-Sevillano, J. J.; Calero, S. Ammonia and Water in Zeolites: Effect of Aluminum Distribution on the Heat of Adsorption. *Sep. Purif. Technol.* **2023**, *306*, 122564. <https://doi.org/10.1016/j.seppur.2022.122564>.
 - (19) Nijem, N.; Fürsich, K.; Bluhm, H.; Leone, S. R.; Gilles, M. K. Ammonia Adsorption and Co-Adsorption with Water in HKUST-1: Spectroscopic Evidence for Cooperative Interactions. *J. Phys. Chem. C* **2015**, *119* (44), 24781–24788. <https://doi.org/10.1021/acs.jpcc.5b05716>.
 - (20) Tan, K.; Ullah, S.; Pandey, H.; Cedeño-Morales, E. M.; Wang, H.; Wang, K.; Zhou, H. C.; Li, J.; Thonhauser, T. Competitive Adsorption of NH₃ and H₂O in Metal-Organic Framework Materials: MOF-74. *Chem. Mater.* **2022**. <https://doi.org/10.1021/acs.chemmater.2c01637>.
 - (21) James, D. W.; Harward, M. E. Competition of NH₃ and H₂O for Adsorption Sites on Clay Minerals. *Soil Sci. Soc. Am. J.* **1964**, *28* (5), 636–640. <https://doi.org/10.2136/sssaj1964.03615995002800050018x>.
 - (22) Atkinson, J. D.; Murray, B. J.; Woodhouse, M. T.; Whale, T. F.; Baustian, K. J.; Carslaw, K. S.; Dobbie, S.; O’Sullivan, D.; Malkin, T. L. The Importance of Feldspar for Ice Nucleation by Mineral Dust in Mixed-Phase Clouds. *Nature* **2013**, *498* (7454), 355–358. <https://doi.org/10.1038/nature12278>.
 - (23) Harrison, A. D.; Whale, T. F.; Carpenter, M. A.; Holden, M. A.; Neve, L.; O’Sullivan, D.; Vergara Temprado, J.; Murray, B. J. Not All Feldspars Are Equal: A Survey of Ice Nucleating Properties across the Feldspar Group of Minerals. *Atmos. Chem. Phys.* **2016**, *16* (17), 10927–10940. <https://doi.org/10.5194/acp-16-10927-2016>.
 - (24) Yakobi-Hancock, J. D.; Ladino, L. A.; Abbatt, J. P. D. Feldspar Minerals as Efficient Deposition Ice Nuclei. *Atmos. Chem. Phys.* **2013**, *13* (22), 11175–11185. <https://doi.org/10.5194/acp-13-11175-2013>.
 - (25) Zolles, T.; Burkart, J.; Häusler, T.; Pummer, B.; Hitzenberger, R.; Grothe, H. Identification of

- Ice Nucleation Active Sites on Feldspar Dust Particles. *J. Phys. Chem. A* **2015**, *119* (11), 2692–2700. <https://doi.org/10.1021/jp509839x>.
- (26) Welti, A.; Lohmann, U.; Kanji, Z. A. Ice Nucleation Properties of K-Feldspar Polymorphs and Plagioclase Feldspars. *Atmos. Chem. Phys.* **2019**, *19* (16), 10901–10918. <https://doi.org/10.5194/acp-19-10901-2019>.
- (27) Holden, M. A.; Campbell, J. M.; Meldrum, F. C.; Murray, B. J.; Christenson, H. K. Active Sites for Ice Nucleation Differ Depending on Nucleation Mode. *Proc. Natl. Acad. Sci. U. S. A.* **2021**, *118* (18), 1–9. <https://doi.org/10.1073/pnas.2022859118>.
- (28) Kaufmann, L.; Marcolli, C.; Hofer, J.; Pinti, V.; Hoyle, C. R.; Peter, T. Ice Nucleation Efficiency of Natural Dust Samples in the Immersion Mode. *Atmos. Chem. Phys.* **2016**, *16* (17), 11177–11206. <https://doi.org/10.5194/acp-16-11177-2016>.
- (29) Pankhurst, M. J. Atmospheric K-Feldspar as a Potential Climate Modulating Agent through Geologic Time. *Geology* **2017**, *45* (4), 379–382. <https://doi.org/10.1130/G38684.1>.
- (30) Freedman, M. A. Potential Sites for Ice Nucleation on Aluminosilicate Clay Minerals and Related Materials. *Journal of Physical Chemistry Letters*. 2015, pp 3850–3858. <https://doi.org/10.1021/acs.jpcclett.5b01326>.
- (31) Franceschi, G.; Conti, A.; Lezuo, L.; Abart, R.; Mittendorfer, F.; Schmid, M.; Diebold, U. How Water Binds to Microcline Feldspar (001). *J. Phys. Chem. Lett.* **2024**, *15* (1), 15–22. <https://doi.org/10.1021/acs.jpcclett.3c03235>.
- (32) Whale, T. F.; Holden, M. A.; Kulak, A. N.; Kim, Y. Y.; Meldrum, F. C.; Christenson, H. K.; Murray, B. J. The Role of Phase Separation and Related Topography in the Exceptional Ice-Nucleating Ability of Alkali Feldspars. *Phys. Chem. Chem. Phys.* **2017**, *19* (46), 31186–31193. <https://doi.org/10.1039/c7cp04898j>.
- (33) Kiselev, A.; Keinert, A.; Gaedeke, T.; Leisner, T.; Sutter, C.; Petrishcheva, E.; Abart, R. Effect of Chemically Induced Fracturing on the Ice Nucleation Activity of Alkali Feldspar. *Atmos. Chem. Phys.* **2021**, *21*, 11801–11814. <https://doi.org/10.5194/acp-21-11801-2021>.
- (34) Holden, M. A.; Whale, T. F.; Tarn, M. D.; Sullivan, D. O.; Walshaw, R. D.; Murray, B. J.; Meldrum, F. C.; Christenson, H. K. High-Speed Imaging of Ice Nucleation in Water Proves the Existence of Active Sites. *Sci. Adv.* **2019**, *5* (2), 1–11.
- (35) Kiselev, A.; Bachmann, F.; Pedevilla, P.; Cox, S. J.; Michaelides, A.; Gerthsen, D.; Leisner, T. Active Sites in Heterogeneous Ice Nucleation—the Example of K-Rich Feldspars. *Science* **2016**, *355* (6323), 367–371. <https://doi.org/10.1126/science.aai8034>.
- (36) Crundwell, F. K. The Mechanism of Dissolution of Minerals in Acidic and Alkaline Solutions: Part IV Equilibrium and near-Equilibrium Behaviour. *Hydrometallurgy* **2015**, *153*, 46–57. <https://doi.org/10.1016/j.hydromet.2015.01.012>.
- (37) Kumar, A.; Marcolli, C.; Peter, T. Ice Nucleation Activity of Silicates and Aluminosilicates in Pure Water and Aqueous Solutions-Part 3: Aluminosilicates. *Atmos. Chem. Phys.* **2019**, *19* (9), 6059–6084. <https://doi.org/10.5194/acp-19-6059-2019>.
- (38) Chardon, E. S.; Livens, F. R.; Vaughan, D. J. Reactions of Feldspar Surfaces with Aqueous Solutions. *Earth-Science Rev.* **2006**, *78* (1–2), 1–26. <https://doi.org/10.1016/J.EARSCIREV.2006.03.002>.
- (39) Murphy, D. M.; Thomson, D. S. Chemical Composition of Single Aerosol Particles at Idaho Hill: Positive Ion Measurements. *J. Geophys. Res. Atmos.* **1997**, *102* (5), 6341–6352. <https://doi.org/10.1029/96jd00858>.
- (40) Anim-Danso, E.; Zhang, Y.; Dhinojwala, A. Surface Charge Affects the Structure of Interfacial Ice. *J. Phys. Chem. C* **2016**, *120* (7), 3741–3748. <https://doi.org/10.1021/acs.jpcc.5b08371>.
- (41) Gonella, G.; Backus, E. H. G.; Nagata, Y.; Bonthuis, D. J.; Loche, P.; Schlaich, A.; Netz, R. R.; Kühnle, A.; McCrum, I. T.; Koper, M. T. M.; Wolf, M.; Winter, B.; Meijer, G.; Campen, R. K.; Bonn, M. Water at Charged Interfaces. *Nat. Rev. Chem.* **2021**, *5* (7), 466–485. <https://doi.org/10.1038/s41570-021-00293-2>.
- (42) Kumar, A.; Marcolli, C.; Luo, B.; Peter, T. Enhanced Ice Nucleation Efficiency of Microcline Immersed in Dilute NH₃ and NH₄⁺-Containing Solutions. *Atmos. Chem. Phys. Discuss.* **2018**, No. January, 1–32. <https://doi.org/10.5194/acp-2018-46>.
- (43) Whale, T. F.; Holden, M. A.; Wilson, T. W.; O’Sullivan, D.; Murray, B. J. The Enhancement

- and Suppression of Immersion Mode Heterogeneous Ice-Nucleation by Solutes. *Chem. Sci.* **2018**, *9* (17), 4142–4151. <https://doi.org/10.1039/c7sc05421a>.
- (44) Chen, L.; Worthy, S. E.; Gu, W.; Bertram, A. K.; Tang, M. The Effects of Ammonium and Ammonium Cations on the Ice Nucleation Activity of K-Feldspar. *J. Geophys. Res. Atmos.* **2023**, *128* (24). <https://doi.org/10.1029/2023JD039971>.
- (45) Wei, X.; Miranda, P. B.; Zhang, C.; Shen, Y. R. Sum-Frequency Spectroscopic Studies of Ice Interfaces. *Phys. Rev. B* **2002**, *66* (8), 085401. <https://doi.org/10.1103/PhysRevB.66.085401>.
- (46) Blow, K.; Whale, T. F.; Quigley, D.; Sosso, G. C. Understanding the Impact of Ammonium Ion Substitutions on Heterogeneous Ice Nucleation. *Faraday Discuss.* **2024**, *249*, 114–132. <https://doi.org/10.1039/d3fd00097d>.
- (47) Whale, T. F. Disordering Effect of the Ammonium Cation Accounts for Anomalous Enhancement of Heterogeneous Ice Nucleation. *J. Chem. Phys.* **2022**, *156* (14). <https://doi.org/10.1063/5.0084635>.
- (48) Franceschi, G.; Kocán, P.; Conti, A.; Brandstetter, S.; Balajka, J.; Sokolović, I.; Valtiner, M.; Mittendorfer, F.; Schmid, M.; Setvín, M.; Diebold, U. Resolving the Intrinsic Short-Range Ordering of K⁺ Ions on Cleaved Muscovite Mica. *Nat. Commun.* **2023**, *14* (1), 208. <https://doi.org/10.1038/s41467-023-35872-y>.
- (49) Kyono, A.; Kimata, M.; Hatta, T. Aluminum Position in Rb-Feldspar as Determined by X-Ray Photoelectron Spectroscopy. *Naturwissenschaften* **2003**, *90* (9), 414–418. <https://doi.org/10.1007/s00114-003-0453-0>.
- (50) Huber, F.; Giessibl, F. J. Low Noise Current Preamplifier for QPlus Sensor Deflection Signal Detection in Atomic Force Microscopy at Room and Low Temperatures. *Rev. Sci. Instrum.* **2017**, *88* (7), 073702. <https://doi.org/10.1063/1.4993737>.
- (51) Schulze Lammers, B.; Yesilpinar, D.; Timmer, A.; Hu, Z.; Ji, W.; Amirjalayer, S.; Fuchs, H.; Mönig, H. Benchmarking Atomically Defined AFM Tips for Chemical-Selective Imaging. *Nanoscale* **2021**, *13* (32), 13617–13623. <https://doi.org/10.1039/d1nr04080d>.
- (52) Sadewasser, S.; Glatzel, T. *Kelvin Probe Force Microscopy*; Sadewasser, S., Glatzel, T., Eds.; Springer Series in Surface Sciences; Springer International Publishing: Cham, 2012; Vol. 48. <https://doi.org/10.1007/978-3-642-22566-6>.
- (53) Kresse, G.; Hafner, J. Ab Initio Molecular Dynamics for Liquid Metals. *Phys. Rev. B* **1993**, *47* (1), 558–561. <https://doi.org/10.1103/PhysRevB.47.558>.
- (54) Kresse, G.; Furthmüller, J. Efficiency of Ab-Initio Total Energy Calculations for Metals and Semiconductors Using a Plane-Wave Basis Set. *Comput. Mater. Sci.* **1996**, *6* (1), 15–50. [https://doi.org/10.1016/0927-0256\(96\)00008-0](https://doi.org/10.1016/0927-0256(96)00008-0).
- (55) Ehlert, S.; Huniar, U.; Ning, J.; Furness, J. W.; Sun, J.; Kaplan, A. D.; Perdew, J. P.; Brandenburg, J. G. R²SCAN-D4: Dispersion Corrected Meta-Generalized Gradient Approximation for General Chemical Applications. *J. Chem. Phys.* **2021**, *154* (6), 61101. <https://doi.org/10.1063/5.0041008>.
- (56) Hapala, P.; Kichin, G.; Wagner, C.; Tautz, F. S.; Temirov, R.; Jelínek, P. Mechanism of High-Resolution STM/AFM Imaging with Functionalized Tips. *Phys. Rev. B* **2014**, *90* (8), 85421. <https://doi.org/10.1103/PhysRevB.90.085421>.
- (57) Hapala, P.; Temirov, R.; Tautz, F. S.; Jelínek, P. Origin of High-Resolution IETS-STM Images of Organic Molecules with Functionalized Tips. *Phys. Rev. Lett.* **2014**, *113* (22), 226101. <https://doi.org/10.1103/PhysRevLett.113.226101>.
- (58) Pérez Ramírez, L.; Gallet, J. J.; Bournel, F.; Lim, F.; Carniato, S.; Rochet, F.; Yazyev, O. V.; Pasquarello, A.; Magnano, E.; Bondino, F. Hydrogen Bonding of Ammonia with (H,OH)-Si(001) Revealed by Experimental and Ab Initio Photoelectron Spectroscopy. *J. Phys. Chem. A* **2020**, *124* (26), 5378–5388. <https://doi.org/10.1021/acs.jpca.0c03458>.
- (59) Landmesser, H.; Kosslick, H.; Storek, W.; Fricke, R. Interior Surface Hydroxyl Groups in Ordered Mesoporous Silicates. *Solid State Ionics* **1997**, *103*, 271–277. [https://doi.org/10.1016/S0167-2738\(97\)84042-8](https://doi.org/10.1016/S0167-2738(97)84042-8).
- (60) Guimon, C.; Gervasini, A.; Auroux, A. XPS Study of the Adsorption of SO₂ and NH₃ over Supported Tin Dioxide Catalysts Used in de-NO_x Catalytic Reaction. *J. Phys. Chem. B* **2001**, *105* (42), 10316–10325. <https://doi.org/10.1021/jp0108869>.

This article has been published in The Journal of Chemical Physics 160, 164312 (2024), doi: 10.1063/5.0202573. The published version is available at: <https://pubs.aip.org/aip/jcp/article/160/16/164312/3284893/NH3-adsorption-and-competition-with-H2O-on-a>.

Supplementary Information for

NH₃ adsorption and competition with H₂O on a hydroxylated aluminosilicate surface

Giada Franceschi,^{*1} Andrea Conti,¹ Luca Lezuo,¹ Rainer Abart,² Florian Mittendorfer,¹
Michael Schmid,¹ Ulrike Diebold¹

¹Institute of Applied Physics, TU Wien, 1040 Vienna, Austria

²Department of Lithospheric Research, Universität Wien, 1090 Vienna, Austria

*Corresponding author. Email: franceschi@iap.tuwien.ac.at

This file includes:

Section S1: AFM images at different tip-sample distances

Section S2: Dosing H₂O directly on the hydroxylated surface

Section S3: XPS spectra

Supplementary References

Section S1: AFM images at different tip-sample distances

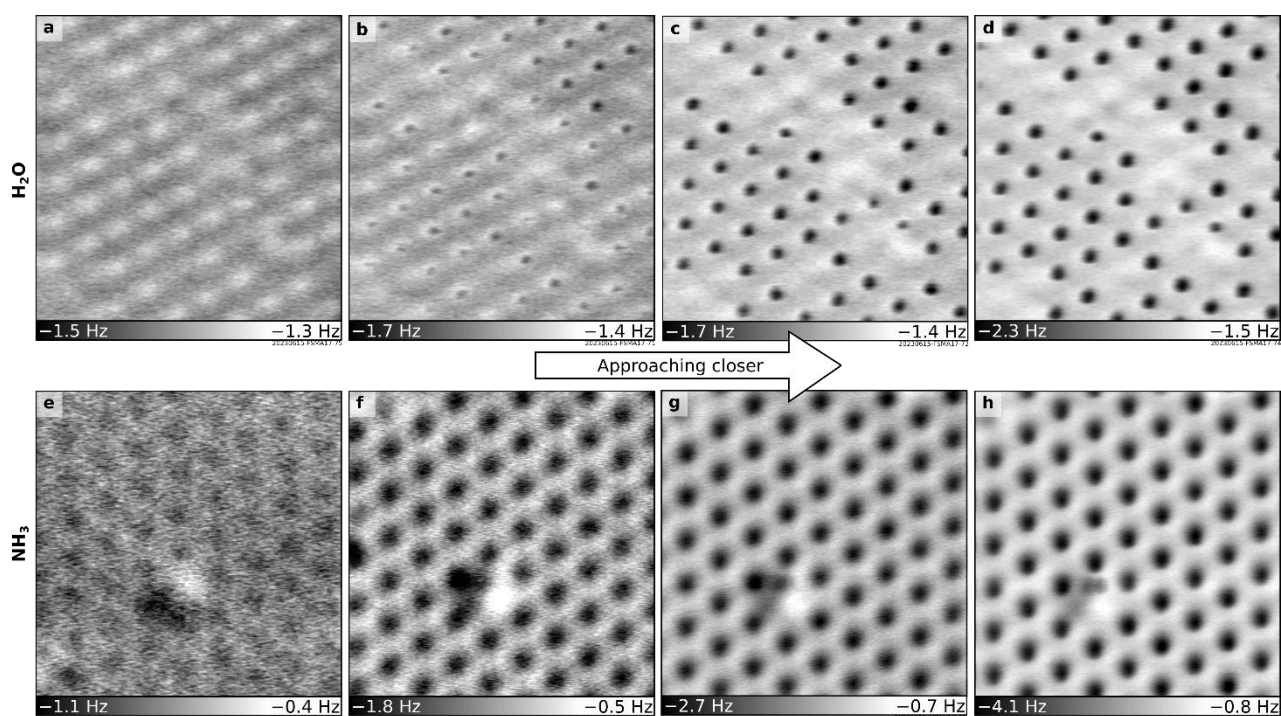


Figure S1. AFM images of H₂O (a–d) and NH₃ (e–h) dosed at 100 K on a hydroxylated microcline (001) surface at decreasing tip-sample distance.

Figures S1a–d show the appearance of H₂O species with an almost full coverage over a hydroxylated (001) microcline surface. From afar, the species appear bright. At closer tip-sample distances, a small dark dot appears at the center of each bright feature. The dot becomes more pronounced as the tip approaches closer. On the other hand, NH₃ species have a much smoother appearance as a function of the tip-sample distance (Figs. S1e–h). Such behavior is also present when the two species coexist on the surface, and allows to distinguish them.

Section S2: Dosing H₂O directly on the hydroxylated surface

Figure S2 shows the appearance of the hydroxylated microcline surface after a nominal dose of 2.5 H₂O/u.c. at 100 K. Most of the surface (brighter contrast) consists of the structure presented in Fig. 1b of the main text, i.e., with 1 H₂O/u.c. H-bonded to two proximate silanol and aluminol groups. The top part of the image is decorated instead with 2D clusters of dark (attractive) features, assigned to H₂O islands. Such islands grow bigger with increasing water coverage until they cover the entire surface (without making 3D clusters). Different from the water islands shown in Fig. 3, obtained by dosing H₂O onto a surface pre-dosed with NH₃, the water islands shown in Fig. S2 display internal short-range ordering. Note that the areal coverage obtained with a nominal dose of 2.5 H₂O/u.c. is significantly larger here compared to

the one obtained on the surface pre-dosed with NH_3 (Fig. 3a of the main text), consistent with the XPS intensities shown in Fig. 2a in the main text.

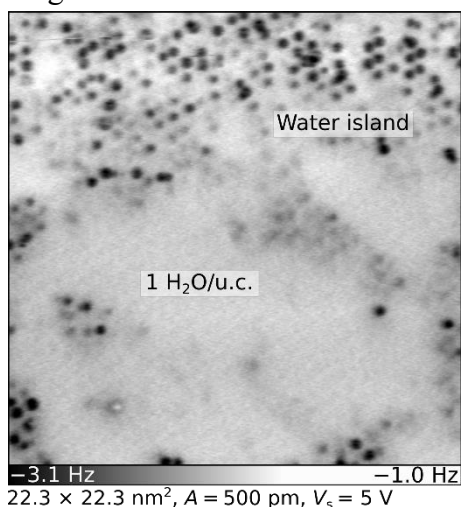


Figure S2. AFM image of the hydroxylated microcline (001) surface exposed to a nominal dose of $2.5 \text{ H}_2\text{O}/\text{u.c.}$ at 100 K.

Section S3: XPS spectra

The details of fitting the O $1s$ peaks are discussed in depth in Ref. 1, and repeated below for convenience. The O $1s$ peak of the cleaved surface was fit by comparing spectra acquired under normal and grazing emission. The normal-emission spectrum was fit by component 1 alone. Fitting the grazing-emission spectrum required component 2 in addition. Component 2 is assigned to surface OH species that saturate the surface at room temperature. Increasing amounts of H_2O at 100 K induced the growth of a third component, which is assigned to molecular H_2O . Its position and FWHM were determined from high-dose experiments, which were then constrained to fit the lower doses. For the fits of the low-temperature water experiments, the intensity ratio of components 1 and 2 was constrained to the value found on the cleaved surface. This is based on the assumption that molecular H_2O grows onto the fully hydroxylated surface. Table S1 summarizes the relevant fitting parameters.

Table S1. Details about the XPS fitting components. The shape (LA=asymmetric Lorentzian), full-width half maximum, and position were constrained for all peaks.

	Identifier	Shape	FWHM	Position (eV)	Area
O $1s$ 1	O $1s$ cleaved	LA(1.53,243)	2.24	532.30	Free
O $1s$ 2	OH cleaved	LA(1.53,243)	2.5	(O $1s$ 1) + 0.60	(Area O $1s$ 1) \times 0.117 (for molecular H_2O dosing)
O $1s$ 3	H_2O	LA(1.43,243)	2.2	(O $1s$ 1) + 1.20	Free
N $1s$	N $1s$	LA(1,253)	2.3	400.4	Free

Figure S3 shows the evolution of the N $1s$ XPS peak upon dosing NH_3 on the hydroxylated microcline surface at 100 K. The peak intensity (Fig. S3a) steadily increases up to a nominal dose of $\approx 3 \text{ NH}_3$ molecules per unit cell, after which it saturates (Fig. S3b).

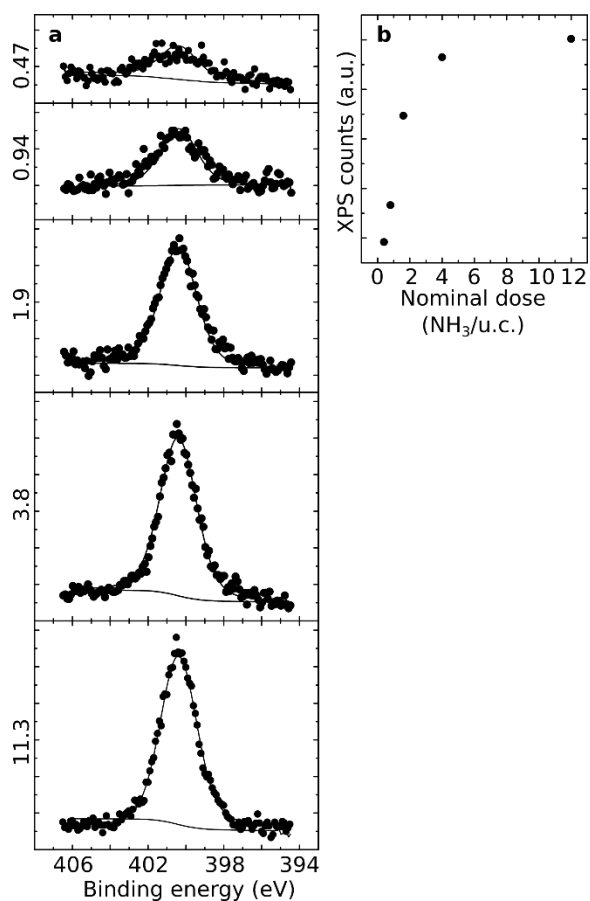


Figure S3. Evolution of the N 1s peak as a function of NH₃ dose at 100 K. (a) Experimental data (circles) and fits (solid lines) of the N 1s peak as a function of the nominal NH₃ dose, expressed as number of NH₃ molecules per unit cell (numbers at the left). (b) Plot of the corresponding intensities. For all spectra: Al K α radiation, 1486.61 eV, pass energy 20 eV, 70° grazing emission. The binding energy axis was adjusted to account for charging (see Methods).

Supplementary References

- (1) Franceschi, G.; Conti, A.; Lezuo, L.; Abart, R.; Mittendorfer, F.; Schmid, M.; Diebold, U. How Water Binds to Microcline Feldspar (001). *J. Phys. Chem. Lett.* **2024**, *15* (1), 15–22. <https://doi.org/10.1021/acs.jpcllett.3c03235>.